Evidence for fault weakness and fluid flow within an active low-angle normal fault

J. S. Floyd*, J. C. Mutter*†, A. M. Goodliffe‡ & B. Taylor‡

** Lamont-Doherty Earth Observatory, Columbia University, Palisades, New York 10964; and Department of Earth and Environmental Sciences, Columbia University; and † Columbia Earth Institute, Columbia University, New York 10027, USA*

‡ School of Ocean and Earth Science and Technology, University of Hawaii, Honolulu, Hawaii 96822, USA

Determining the composition and physical properties of shallow-dipping, active normal faults (dips < 35° with respect to the horizontal) is important for understanding how such faults slip under low resolved shear stress and accommodate significant extension of the crust and lithosphere. Seismic reflection images[1] and earthquake source parameters[2] show that a magnitude 6.2 earthquake occurred at about 5 km depth on or close to a normal fault with a dip of 25–30° located ahead of a propagating spreading centre in the Woodlark basin. Here we present results from a genetic algorithm inversion of seismic reflection data, which shows that the fault at 4–5 km depth contains a 33-m-thick layer with seismic velocities of about 4.3 km s^{-1}, which we interpret to be composed of serpentinite fault gouge. Isolated zones exhibit velocities as low as ~1.7 km s^{-1} with high porosities, which we suggest are maintained by high fluid pressures. We propose that hydrothermal fluid flow, possibly driven by a deep magmatic heat source, and high extensional stresses ahead of the ridge tip have created conditions for fault weakness and strain localization on the low-angle normal fault.

We use multichannel seismic (MCS) reflection data acquired aboard the RV *Maurice Ewing* during a 1995 survey and drilling results from Ocean Drilling Program (ODP) Leg 180 (refs 3 and 4; Fig. 1). MCS profiles[1,4] reveal a normal fault that maintains a dip of 25–30° to about 9 km depth and an offset of 10–12 km between the sedimented hanging wall and the Moresby seamount footwall, which is composed of Palaeocene arc-ophiolite gabbro and dolerite[3,5]. Faulting and uplift of Moresby seamount is estimated to have begun within the last 3.5 Myr, based on the first occurrence of metamorphic talus found in the downdropped hanging wall at ODP Site 1108 and an abrupt increase in sedimentation rate that indicates rapid subsidence of the northern margin at this time[3]. This fault is one of the major structures on which continental extension appears to be localized. The close proximity of the fault to the

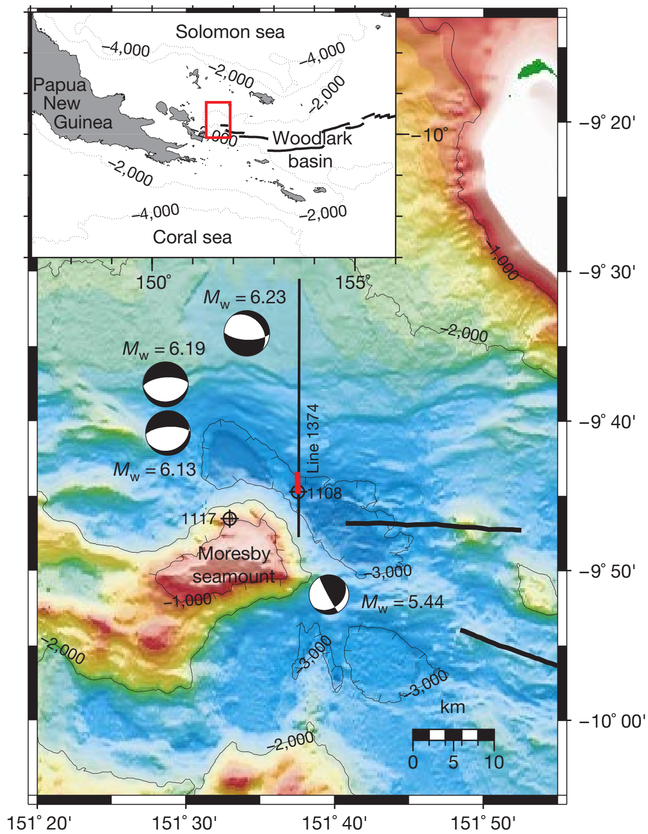

Figure 1 Bathymetry map of the study area showing the location of RV *Maurice Ewing* EW9510 multichannel seismic (MCS) reflection line 1374. The portion of the MCS line 1374 used in the inversion is marked in red. The ODP Leg 180 drill sites 1108 and 1117 discussed in the text are marked[3]. Earthquake focal mechanisms[2] shown include the M_w 6.23 event which occurred on or near the low-angle normal fault on the northern flank of Moresby seamount. Heavy black lines mark the location of the ridge axis interpreted from side-scan sonar data[23]. Bathymetry contours are given in units of metres. Inset, regional map showing the location of the study area (red box).

spreading ridge tip (Fig. 1) suggests that this will be the last continental fault to form before complete break-up creates new oceanic lithosphere.

Anderson–Byerlee fault mechanics predicts that normal faults should form at dips greater than 45° (ref. 6). Faults may rotate to shallower dips and continue to slip, but for reasonable values of the coefficient of friction[7], they will 'lock up' before reaching 30°. This assumes, however, that the stress field within the fault zone is the same as that outside the fault zone. Rice[8] and others (for example, ref. 9) have shown that a different stress state will exist if the fault contains mechanically weak gouge or pore fluids at near-lithostatic pressures. As seismic velocities are a function of the density, porosity and elastic moduli of the material through which seismic waves propagate, variations in seismic velocity can be used to constrain the composition, physical properties and, hence, the strength of the fault zone.

We investigated the conditions on the imaged fault plane at depth by using a genetic algorithm[10] to invert for the compressional (P) wave velocity and thickness of an approximately 2.15-km-long segment of the fault from the time-migrated MCS line 1374 (Fig. 2). Line 1374 is located on the northeast flank of Moresby seamount and contains the clearest image of the fault compared to other MCS lines in the region which are complicated by out-of-plane reflections from Moresby seamount. The genetic algorithm finds the best-fitting velocity model by allowing a population of starting models to evolve according to the darwinian principle of 'survival of the fittest' (see Methods). We inverted every fifth seismogram spaced 50 m apart between common midpoints (CMPs) 1480 and 1630 between 4.90 and 5.45 s (approximately 4.15 to 5.12 km depth). The theoretical vertical resolution[11] of our MCS data is approximately 12.5 m. The inversion results define a fault zone consisting of a layer 33.4 ± 5.7 m thick with P-wave velocities of 4.3 ± 0.22 km s^{-1} throughout most of the fault and 1.74 ± 0.24 km s^{-1} in isolated sections along the deeper portion of the fault plane (Fig. 3). We also tested a three-layer model to evaluate possible vertical variations in the fault zone velocity. The three-layer model shows a similar velocity structure that contains only minor vertical variations, with the exception of a positive velocity gradient around CMP 1515 and thin 3.0–4.0 km s^{-1} layers interleaved within the low-velocity zones between CMPs 1560 and 1630.

To examine more closely the low-velocity sections of the fault, we analysed the fault reflection amplitude variation with offset (AVO) in CMP gathers 1500 and 1600 (Fig. 4), which are representative of high- and low-velocity sections of the fault zone. At CMP 1500 the P-wave velocity increase at the sediment–fault interface produces a positive polarity reflection at near offsets, whereas at CMP 1600 the P-wave velocity decrease produces a negative polarity reflection. With increasing offset fault reflection amplitudes of both CMP gathers decrease, which corresponds to a decrease in Poisson's ratio across the interface as shown by the Zoeppritz equations[12,13]. Poisson's ratio is a positive, nonlinear function of the ratio between P- and S-wave velocities. The decrease in Poisson's ratio in the low-velocity zones indicates that the P-wave velocity decreases with respect to the S-wave velocity across the interface. This result is best explained by the presence of fluids in the fault zone: because S-waves do not travel through fluids, the S-wave velocity may decrease owing to lower bulk density, but P-wave velocity is reduced by both lower bulk density and slower travel paths through pore fluids. By cross-plotting the zero-offset amplitude (intercept) and rate of change of amplitude with offset (gradient) of the fault zone reflection for CMPs 1480–1630 (ref. 13; Fig. 2), we find that fault reflections with negative intercept and gradient values consistently correlate with low-velocity zones identified by our genetic algorithm inversion (Fig. 3).

The composition of the fault zone material is limited to rock derived from either the sedimentary hanging wall or the gabbroic footwall. The sediment velocity is too low (3 km s^{-1}, Fig. 3) to account for the ~4.3 km s^{-1} fault zone velocity, therefore we infer that the fault zone is composed of material derived from the footwall gabbro that has been reduced in velocity by shearing and hydrothermal alteration. Fluid-assisted deformation of mafic

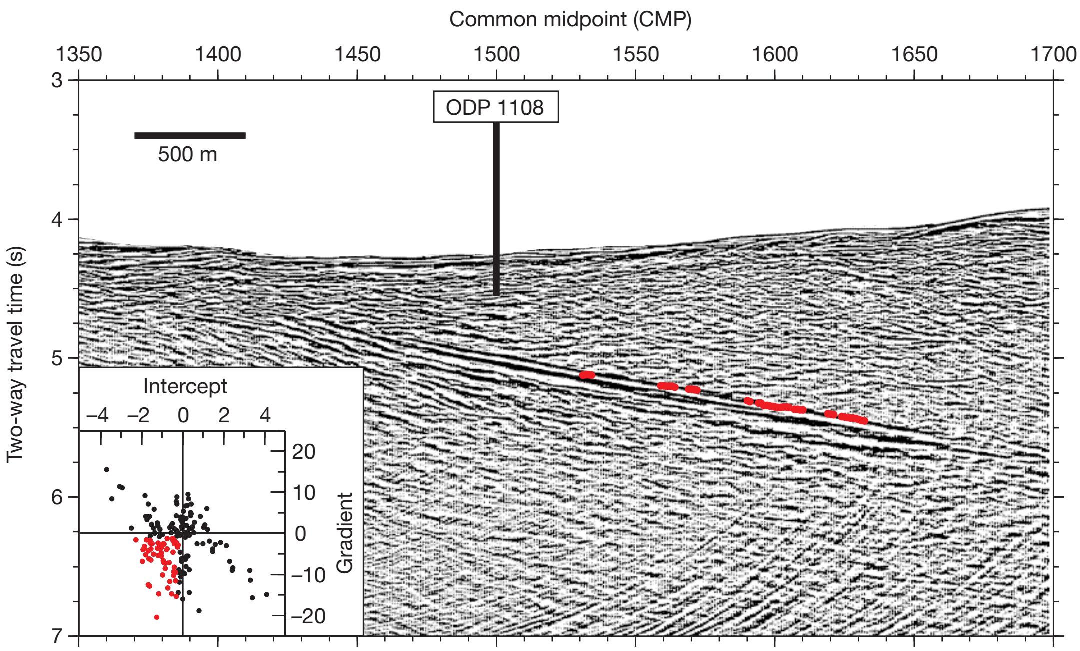

Figure 2 Multichannel seismic line 1374. Processing steps included normal moveout, predictive deconvolution, time migration and spherical spreading correction. ODP Leg 180 site 1108 penetrated to a depth of 485.2 metres below sea floor (m.b.s.f.) and is shown reaching to its approximate depth in units of two-way travel time. CMP spacing is 12.5 m. Inset, intercept and gradient crossplot calculated by fitting the amplitude variation with offset (AVO) values of the fault reflection to the linearized form of the Zoeppritz equations[13] for CMPs 1480 to 1630. Fault reflections with AVO values that fall within the quadrant with negative intercept and negative gradient are marked in red in the crossplot and at the corresponding CMP locations on the seismic profile.

igneous rocks commonly forms serpentinite, which is widely found in oceanic shear zones along transform and normal faults on mid-ocean ridges[14]. At ODP Site 1117, we recovered approximately 4 m of serpentinized material containing talc, serpentine polymorphs, chlorite and magnetite on top of Moresby seamount, which we interpreted to be fault gouge[3] (Fig. 1). Drilling results confirmed that the northern flank of Moresby seamount is an exposed, ~100-m-thick shear zone that has undergone hydrothermal alteration under greenschist facies metamorphism. We suggest that the fault zone imaged by MCS line 1374 similarly contains serpentinite fault gouge and consider the ~35 m layer determined by seismic waveform inversion to represent only the most deformed and altered material between the offset crustal blocks.

Shipboard laboratory measurements of the serpentinite gouge give a velocity of 2.0 km s^{-1} and a porosity of 30%. Assuming that the low-velocity zones contain material that is similar to the fault gouge recovered at ODP Site 1117, we estimate that a porosity of 61% is needed to explain the decrease in velocity to 1.74 km s^{-1} (ref. 15). This is a minimum value—if higher-velocity material were mixed into the gouge, a higher porosity would be required. Laboratory studies show that only a 10% porosity increase in the fault gouge can be explained by shear deformation[16]. Seismic anisotropy due to shear would lower the overall velocity of the fault zone, but would be expected to be uniform in the direction of slip and would not explain the presence of isolated low-velocity zones. On the basis of our evidence for fluids from genetic algorithm inversion and AVO analysis, we propose that the calculated high-porosity value is best explained by the presence of high pore-fluid pressures in the fault zone. Fluid pressures must be near-lithostatic, otherwise the pore spaces would close under the weight of the overburden.

Evidence for high fluid pressures from our seismic data analysis, together with the occurrence of serpentinite recovered up-dip on the same fault by ODP drilling, suggests that hydrothermal fluid flow may be actively weakening the fault zone. The composition of the fault material and its structural relationship to the nearby spreading ridge lead us to propose that the tectonics of the low-angle normal fault may be explained by analogy to normal detachments flanking inside corner highs of slow- (<25–30 mm yr^{-1}) to intermediate-rate (25–40 mm yr^{-1}) spreading ridges[14,17]. The tip of the Woodlark ridge, which is spreading at a rate of 34 mm yr^{-1} at 151.5° E (ref. 18), is currently located in a right-stepping offset configuration with respect to the normal fault, placing Moresby seamount at a potential inside-corner position. Structural features that are common to inside-corner highs and Moresby seamount include an asymmetric rift axis; a shallowly dipping (20–40°), corrugated[19] slip surface; a rounded dome shape; and a deep nodal basin opposing the elevated footwall[14] (Fig. 1). Larger-scale tectonic elements that are common to the Woodlark rift and oceanic propagators were recognized by Mutter *et al.*[20]. Studies of normal detachments flanking inside corner highs show that they occur at the ends of ridge segments where magma supply is low and

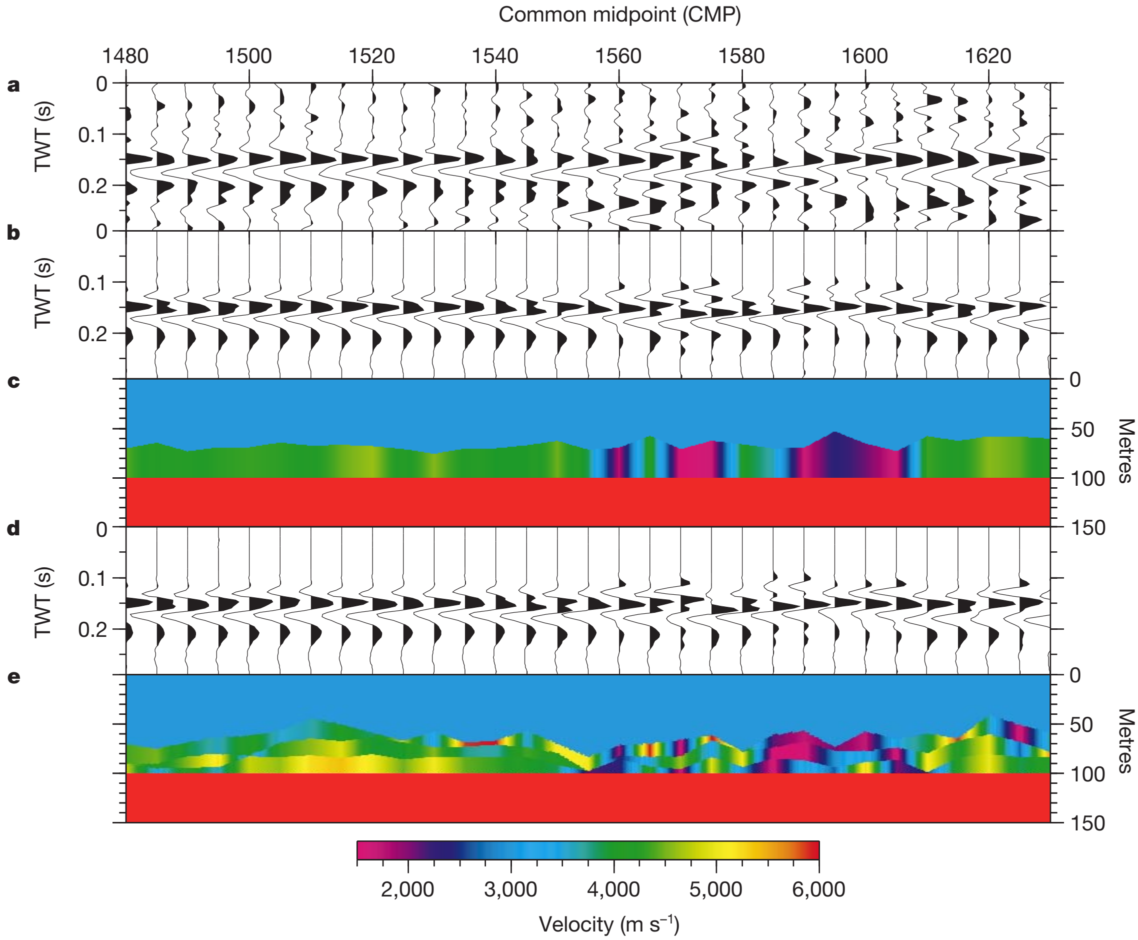

Figure 3 Velocity structure of the fault zone flattened along the fault–basement contact determined by genetic algorithm inversion of every fifth trace from CMPs 1480 to 1630 of MCS line 1374. **a**, Original MCS seismograms flattened at the first positive-polarity peak at or slightly above the fault reflection. **b**, Best-fit synthetic seismograms for the single-layer velocity model (**c**). **d**, Best-fit synthetic seismograms for the three-layer velocity model (**e**). Constant velocities of 3.0 km s^{-1} and 6.0 km s^{-1} were used in the inversion for the sedimentary hanging wall and gabbroic footwall, respectively. TWT, two-way travel time.

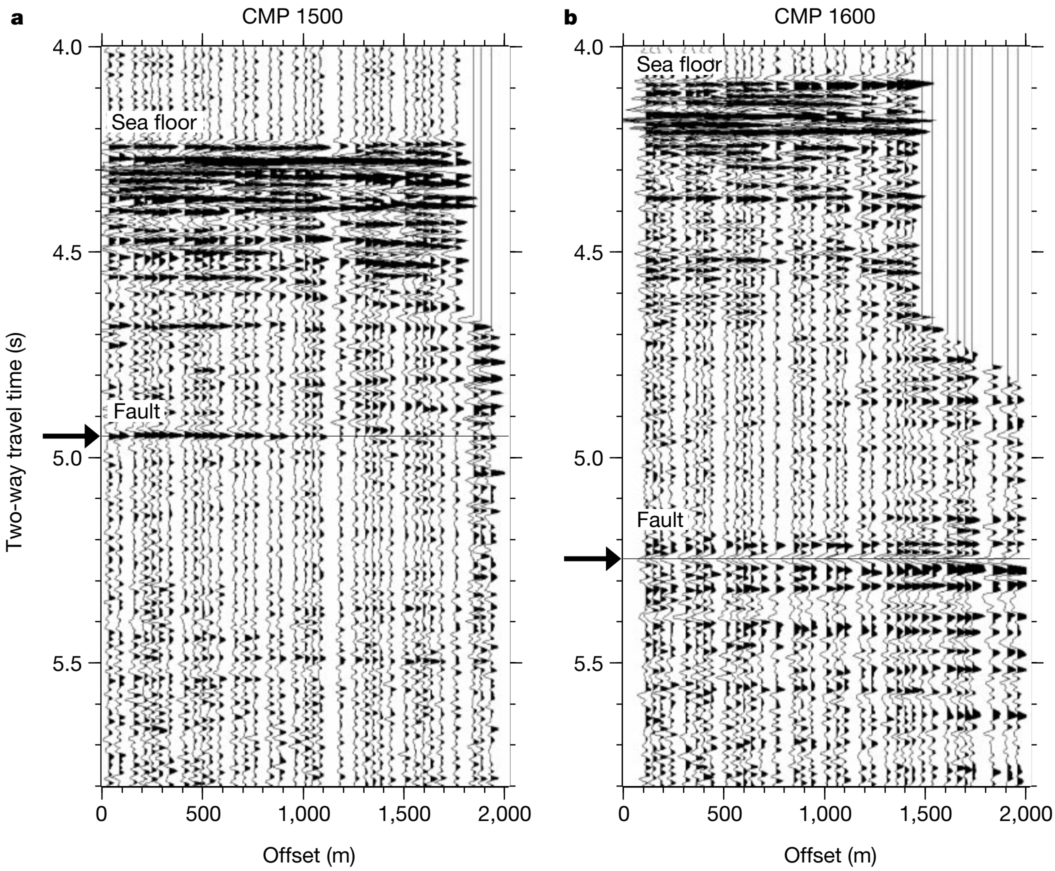

Figure 4 Normal-moveout-corrected CMP gathers 1500 (**a**) and 1600 (**b**) from MCS line 1374. Arrows mark the location of the positive-polarity fault reflection at CMP 1500 and the negative-polarity reflection at CMP 1600. The fault reflection in CMP 1500 (**a**) decreases with offset and exhibits a polarity reversal at 1.2 km, while the fault reflection in CMP 1600 (**b**) that images the low-velocity zone becomes increasingly negative for all offsets.

spreading is accommodated by tectonic extension[14]. ODP Leg 180 borehole temperature measurements at Site 1108 revealed a thermal gradient up to 100 °C km^{-1} in the hanging wall ahead of the ridge tip[3]. We suggest that the role of the Woodlark ridge is to provide high extensional stress and a magmatic heat source that drives convective hydrothermal fluid flow through the fault zone, which weakens the fault by hydrothermal alteration and development of high fluid pressures. In this way, the composition and physical properties of the fault zone and the processes by which these elements form not only provide conditions favourable for normal faulting at low angles, but may also fundamentally control the localization of strain on low-angle normal detachments at the rifting–spreading transition. □

Methods

Genetic algorithms are used in many areas of science to solve nonlinear inverse problems[21]. The genetic algorithm begins with a random population of starting models that undergo a process of selection, crossover and mutation in which the best-fitting models stand the greatest likelihood of being reproduced and passed on to the next generation. The efficiency of the algorithm lies in the fact that unpromising areas of the model space are quickly left behind in favour of more promising areas that are explored in later generations. The process is stopped when the population converges to a maximum fitness value and does not improve with more iterations.

We used the root-mean-square (r.m.s.) error between the synthetic and recorded seismograms as the fitness function to be minimized by the genetic algorithm. Normal incidence synthetic seismogram calculations included the effects of interbed multiples, seismic attenuation and dispersion[22]. The quality factor (Q) of the sediments overlying the fault zone was estimated from MCS data using the spectral ratio method and was found to follow an expected exponential trend with depth from 20 to 65. ODP Leg 180 shipboard measurements[3] and MCS interval velocities provided constraints on the sediment and gabbro velocities, which were held constant in the inversion at 3.0 and 6.0 km s^{-1}, respectively. Starting models were chosen randomly from velocity and thickness combinations between 1.5 km s^{-1} (the velocity of water) to 6.0 km s^{-1} (the velocity of undeformed gabbro) and 0 to 50 m, respectively. Initial tests showed that the best-fit layer thickness was less than 50 m; therefore, the upper layer thickness boundary was set to this value to speed convergence. The starting population for the single-layer model consisted of 100 randomly generated models that evolved over 50 generations to test a total of 5,000 models for each CMP. For the three-layer model, the initial population consisted of 100 individuals that evolved over 100 generations to test 10,000 models for each CMP. The use of one-dimensional seismograms to model a two- or even three-dimensional structure is clearly a simplification; however, this approach is justified by the shallow dip and planar structure of the fault within the modelled region and provides a computational advantage that allowed many more models to be tested. AVO analysis of the CMP gathers provided an independent approach to determination of fault properties that were found to be consistent with the genetic algorithm results and verified that the low-velocity zones are not artefacts of either MCS data processing or the genetic algorithm inversion method.

Received 15 December 2000; accepted 19 April 2001.

1. Mutter, J. C., Mutter, C. Z., Abers, G. & Fang, J. Seismic images of low-angle normal faults in the western Woodlark Basin where continental extension yields to seafloor spreading. *Eos Trans AGU* **74,** 412 (1993).
2. Abers, G. A., Mutter, C. Z. & Fang, J. Shallow dips of normal faults during rapid extension: Earthquakes and normal faults in the Woodlark-D'Entrecasteaux rift system, Papua New Guinea. *J. Geophys. Res.* **102,** 15301–15317 (1997).
3. Taylor, B. *et al. Proc. ODP Init. Rep.* [CD-ROM] **180**, (Ocean Drilling Program, College Station, 1999).
4. Taylor, B., Mutter, C., Goodliffe, A. & Fang, J. Active continental extension: the Woodlark Basin. *JOI/USSAC Newsl.* **9,** 1–4 (1996).
5. Davies, H. L. & Smith, I. E. Geology of Eastern Papua. *Geol. Soc. Am. Bull.* **82,** 3299–3312 (1971).
6. Anderson, E. M. *The Dynamics of Faulting and Dyke Formation with Application to Britain* (Oliver and Boyd, Edinburgh, 1942).
7. Byerlee, J. D. Friction of Rocks. *Pure Appl. Geophys.* **116,** 615–626 (1978).
8. Rice, J. R. in *Fault Mechanics and Transport Properties of Rock* (eds Evans, B. & Wong, T.-F.) 475–503 (Academic, San Diego, 1992).
9. Byerlee, J. D. Friction, overpressure and fault normal compression. *Geophys. Res. Lett.* **17,** 2109–2112 (1990).
10. Sen, M. K. & Stoffa, P. L. Rapid sampling of model space using genetic algorithms: examples from seismic waveform inversion. *Geophys. J. Int.* **108,** 281–292 (1992).
11. Widess, M. B. How thin is a thin bed? *Geophysics* **49,** 1637–1648 (1984).
12. Ostrander, W. J. Plane-wave reflection coefficients for gas sands at nonnormal angles of incidence. *Geophysics* **49,** 1637–1648 (1984).

13. Shuey, R. T. A simpli®cation of the Zoeppritz equations. Geophysics 50, 609±614 (1985).
14. Tucholke, B. E. & Lin, J. A geological model for the structure of ridge segments in slow spreading ocean crust. J. Geophys. Res. 99, 11937±11958 (1994).
15. Wyllie, M. R. J., Gregory, A. R. & Gardner, G. H. F. An experimental investigation of factors affecting elastic wave velocities in porous media. Geophysics 23, 459±493 (1958).
16. Marone, C., Raleigh, C. B. & Scholz, C. H. Frictional behavior and constitutive modeling of simulated fault gouge. J. Geophys. Res. 95, 7007±7025 (1996).
17. Mutter, J. C. & Karson, J. A. Structural processes at slow-spreading ridges. Science 257, 627±634 (1992).
18. Taylor, B., Goodliffe, A. M. & Martinez, F. How continents break up: Insights from Papua New Guinea. J. Geophys. Res. 104, 7497±7512 (1999).
19. Tucholke, B. E., Lin, J. & Kleinrock, M. C. Megamullions and mullion structure de®ning oceanic metamorphic core complexes on the Mid-Atlantic Ridge. J. Geophys. Res. 103, 9857±9866 (1998).
20. Mutter, J. C., Mutter, C. Z. & Fang, J. Analogies to oceanic behaviour in the continental breakup of the western Woodlark Basin. Nature 380, 333±336 (1996).
21. Goldberg, D. E. Genetic Algorithms in Search, Optimization and Machine Learning (Addison-Wesley, Reading, MA, 1989).
22. Ganley, D. C. A method for calculating synthetic seismograms which includes the effects of absorption and dispersion. Geophysics 46, 1100±1107 (1981).
23. Taylor, B., Goodliffe, A., Martinez, F. & Hey, R. Continental rifting and initial sea-¯oor spreading in the Woodlark basin. Nature 374, 534±537 (1995).

Acknowledgements

We thank W. Menke, C. Scholz, S. Carbotte, A. Lerner-Lam and D. Goldberg for helpful discussions and R. Detrick and W. Bosworth for comments that improved this Letter. J.F. and J.M. were supported under a grant from JOI/USSAC. We thank the captain and crew of the RV *Maurice Ewing* for MCS data acquired on EW9510. ODP Leg 180 drilling results used in this study were obtained thanks to the efforts of the captain and crew of the DV *JOIDES Resolution*; A. Klaus and the TAMU scienti®c support staff; co-chiefs P. Houchon and B. Taylor and the ODP Leg 180 Scienti®c Party.

Correspondence and requests for materials should be addressed to J.F. (e-mail: js¯oyd@ldeo.columbia.edu).